scientific reports

Check for updates

OPEN

Tuning structures and catalysis performance of two-dimensional covalent organic frameworks based on copper phthalocyanine building block and phenyl connector

Yuexing Zhang[1]✉, Junhao Peng[1,3], Guangsong Zhang[1,3], Xingguo Zhang[1], Shuai Zhang[1], Qing Li[1], Guanfeng Tian[1], Xiaoli Wang[1], Ping Wu[1] & Xue-Li Chen[2]✉

Based on the experimentally reported stable and conductive two-dimensional covalent organic frameworks with copper phthalocyanine (CuPc) as building block and cyan substituted phenyl as connector (CuCOF-CN) as an electrocatalyst for CO_2 reduction reaction (RR), first principle calculations were performed on CuCOF-CN and its analog with the CN being replaced by H (CuCOF). Comparatively studied on the crystal structures, electronic properties, and CO_2RR performance of the two catalysts found that CuCOF has reduced crystal unit size, more positive charge on Cu and CuPc segments, smaller band gap, and lower reaction barrier for CO_2 RR than CuCOF-CN. CuCOF is proposed to be good potential electrocatalyst with good environment friendliness. The substituent effect and structure-property-performance relationship would help for designing and fabricating new electrocatalysts.

Keywords COF, CO_2 reduction reaction, Copper phthalocyanine, Electrocatalyst, First principle calculation

Increasing energy crisis and global warming problems from carbon dioxide (CO_2) emission have been caused by the utilization of non-renewable fossil fuels and mankind's living requirements[1]. Reducing the CO_2 concentration in the atmosphere therefore is highly desirable by transferring CO_2 to other sustainable energies[2–6]. The thermodynamically stable molecule CO_2 is highly inert and the electrochemical CO_2 reduction (CO_2RR) process is kinetically sluggish requiring very high potential (−1.90V vs.NHE)[7,8] Many different kind of materials have been developed to seek highly efficient, selective and stable electrocatalyst that can reduce the activation energy barrier and expedite the kinetics of CO_2RR[9–11]. Cheap transition metal copper-based catalysts had many advantages and were widely developed[12–17].

Among the catalysts for CO_2 RR, N_4-macrocyclic complexes based molecular electrocatalysts including metal porphyrins, phthalocyanines and their related derivatives have emerged as the promising candidates[18–22]. To solve the problem of the relatively high over-potential due to the poor conductivity and sluggish electron transfer[22], efforts have been tried to either coupling metal phthalocyanines or porphyrins with high conductive carbon nanomaterials or designing highly conjugated system[20,22,23]. A number of two-dimensional (2D) conductive covalent-organic frameworks (COFs) with extensive planar π-conjugation have been shown high electrical conductivity and developed for electrocatalysts[24–27].

Series of metal phthalocyanine based 2D-COFs have been developed recently. Liao et al. reported a stable and conductive 2D-COF with copper phthalocyanine as building block and cyan substituted phenyl as connector (CuCOF-CN) in 2022[28]. CuCOF-CN show good electrocatalytic performance for CO_2 RR to acetate with a single-product Faradaic efficiency (FE) of 90.3(2)% at −0.8 V (vs. RHE) and a current density of 12.5 mA cm^{-2} in 0.1 M $KHCO_3$solution. They also performed theoretical calculation to explain why CuCOF-CN show

[1]Shandong Provincial Key Laboratory of Monocrystalline Silicon Semiconductor Materials and Technology, Shandong Provincial Engineering Research Center of Organic Functional Materials and Green Low-Carbon Technology, Shandong Universities Engineering Research Center of Integrated Circuits Functional Materials and Expanded Applications, College of Chemistry and Chemical Engineering, Dezhou University, Dezhou 253023, P. R. China. [2]Jiangxi Provincial Key Laboratory of Low-Carbon Solid Waste Recycling, School of Geography and Environmental Engineering, Gannan Normal University, Ganzhou 341000, P. R. China. [3]These authors contributed equally to this work. ✉email: zhangyuexing@sdu.edu.cn; xueli089@foxmail.com

different catalysis property from other Cu-based catalyst including copper porphyrin and single-atom copper catalyst. However, the synthesis of CuCOF-CN was time-costing and not economy (it was synthesized by a condensation reaction at 150 ℃ for 3 days under vacuum). The crystal structures of the CuCOF-CN was also not discussed. In addition, the phenyl connector contain two -CN group, which is extremely toxic substance and has great harm to the environment and to human beings. Jiang et al. developed a solvent-free, facile, and fast synthesis strategy for fabricating two fully conjugated Pc-based COFs under ionothermal synthesis for 8 h[29]. One of the COF reported by Jiang et al. show very similar structure as CuCOF-CN reported by Liao et al.[28], with the center metal of CuCOF-CN being changed to zinc and the CN substituents replaced with H (ZnCOF). Despite that the zinc center was not good candidate for catalyst, these COFs show high-performance K^+storage in potassium-ion batteries in terms of the large reversible capacities, excellent rate performance, and long-term cycling stability. Recently and during the preparation of the present work, Chen et al. further improved the synthesis strategy of 2D-COF and synthesized series metal (M = Fe, Co, Ni, Cu, Zn) phthalocyanine based COFs (MCOFs) by a facile trace-solvent-assisted one-pot self-condensation method[30]. Among these MCOFs, NiCOF show excellent sensing properties for various analytes including neurotransmitters, organic pollutants, and heavy metal ions, with high sensitivity and low detection limit of 0.53 to 25.66 nM. However, the catalysis performance of these MCOFs were not reported though CuCOF-CN show good CO_2 RR performance. The influence of CN substitution on crystal structure, electronic properties, and catalytic performance were not clear. Clarifying these questions with a theoretical prospective work would therefore have great significance.

To further clarify the structures and rule of CN on the CO_2 reduction performance, in the present work, we comparatively studied the crystal structures, electronic properties, and CO_2 RR performance of CuCOF-CN and CuCOF through first principle calculations. The substituent effect and structure-property-performance relationship would help for designing and fabricating new electrocatalysts.

Computational methods

The initial crystal structures of CuCOF and CuCOF-CN were built with Device Studio program[31]. Device Studio program provides a number of functions for performing visualization, modeling and simulation. The first principle simulation were performed using DS-PAW software[32]integrated in Device Studio program. The PBE exchange-correlation functional[33]and D3BJ Van der Waals correction[34] were chosen.

Results and discussion

Structures

Figure 1 shows the optimized crystal structures of CuCOF and CuCOF-CN. Their main structure parameters are tabulated in Table 1. Both CuCOF and CuCOF-CN are 2D planar layer structure without any deviation from the 2D plane. The crystals are both *P4/mmm* symmetry with a = b and $\alpha = \beta = \gamma = 90.0^{o}$. To avoid interactions between layers, the c-axis are set to 10.000 Å after involving the vacumm layer. The a and b values of CuCOF-

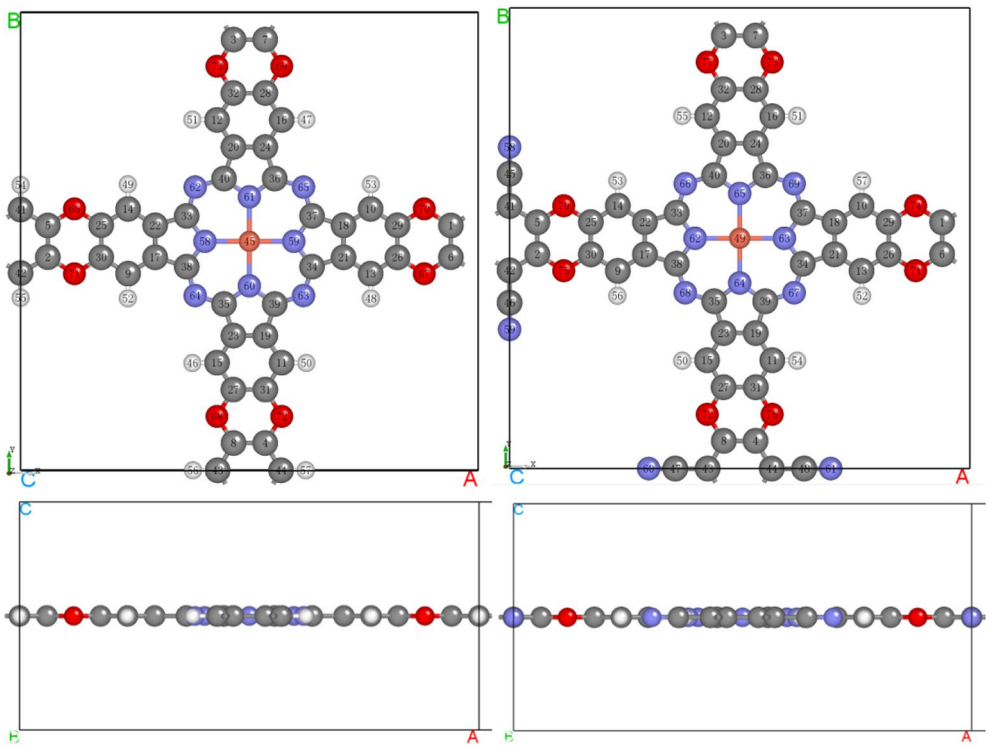

Fig. 1. Top (top) and side view (bottom) of the optimized crystal structures of CuCOF (left) and CuCOF-CN (right). (Red: O, gray: C, blue: N, white: H, coral: Cu).

Parameter	CuCOF	CuCOF-CN
Symmetry group	P4/mmm	P4/mmm
a	20.192	20.197
b	20.192	20.197
c	10.000	10.000
α	90.0	90.0
β	90.0	90.0
γ	90.0	90.0
Cu-N	1.963	1.961
Width(Py)	2.195	2.197
Width(Ph of Pc)	2.381	2.373
Width(C_4O_2)	2.356	2.351
Width(Ph connector)	2.403	2.432
Height(Ph connector)	2.799	2.815

Table 1. Main structure parameters of the optimized crystal of CuCOF and CuCOF-CN (length in Å, angle in °).

CN is somewhat longer than those of CuCOF (20.197 vs. 20.192 Å), indicating that the substitution of H on the phenyl connector in CuCOF with electron-withdrawing CN group slightly enlarge the cell size of the COF crystals. More detail, the Cu-N bonds and the width of phenyl ring of phthalocyanine and the neighbour C_4O_2 ring all reduce, while the pyrrole ring of Pc and phenyl connector enlarge largely. In addition, CN substitution also induces the increase of height of phenyl connector. The different changes suggest that the electron density in the COF is redistributed due to the involving of electron-withdrawing CN groups in CuCOF-CN, which in turn would induce their different electrocatalytic performance.

Bader charge

The introduction of electron-withdrawing CN groups would induce the redistribution of electrons. Table 2 shows the calculated Bader charge on each atom of CuCOF and CuCOF-CN as well as the change of Bader charge upon CN substitution. The H atoms of phenyl connector in CuCOF have Bader charge of 0.112 e, while the CN substituents in CuCOF-CN have Bader charge of −0.435 e. The Bader charge on C connected with H or CN changes from negative − 0.179 in CuCOF to positive 1.272 e in CuCOF-CN. The phenyl connector (in a or b direction) and its neighbour four O atoms in CuCOF totally contain Bader charge of −2.068 e. Since there are two connector in each crystal cell and the crystal is neutral, the remaining CuPc segment in CuCOF thus has Bader charge of 4.136 e. For CuCOF-CN, the Bader charge on each connector and CuPc segment increases to −2.452 and 4.904 e, respectively. These results indicate that electron transfer from CuPc segment to the connector and CN substitution on connector increases the electron transfer extent. Considering the Barder charge on Cu atom, Cu in CuCOF however has larger value than that in CuCOF-CN, 1.101 vs. 0.913 e. Large charge on Cu is advantage for CO_2 RR reaction.

Band structure

Figure 2 shows the calculated projected band structure of CuCOF and CuCOF-CN between − 2 and 2 eV. The calculated Fermi energies of CuCOF and CuCOF-CN are − 3.04 and − 3.40 eV, respectively. The lower Fermi energy upon electron-withdrawing CN substitution is consistent with the common knowledge that electron-withdrawing groups would lower the orbital energy for molecule. Worth noting that when aligning the Fermi energy of both CuCOF and CuCOF-CN to 0 eV, the bands of CuCOF-CN appear above the corresponding bands of CuCOF. For CuCOF, the band around 0 eV is mainly composed from the p orbital of N atoms and d orbital of Cu. The band around − 0.5 eV of CuCOF including the p orbital of both C and O atoms, while that below it is mainly from C p orbital. Band around − 1.5 eV have large contribution from O p orbital in addition to major content from C p orbital. The bands around − 1.7 eV are composed from p orbital of both C and N. Similarly, the conduction band around 0.7 eV are also composed from p orbital of both C and N atoms. The shape and composition of band structures of CuCOF-CN are very similar to those of CuCOF. Some new bands appear around 1.6 eV in CuCOF-CN, which are composed of p orbitals of C and N and may due to the contribution of the CN substituents. The band gap from conducting band bottom to valence band top for CuCOF is 0.69 eV, much smaller than the gap for CuCOF-CN (0.88 eV), indicating that the conductivity of CuCOF is better than CuCOF-CN. Good conductivity is advantage for improving the electrocatalytic performance.

Density of states

The projected density of states (PDOS) of CuCOF and CuCOF-CN are shown in Fig. 3. In line with the assignments in Band structure section, PDOS peak around 0 eV are mainly contributed from the Cu d orbital and N p orbital, while the other peaks are attributed from the p orbital of C, N, and O atoms. The PDOS peaks of CuCOF are stronger than those of CuCOF-CN, indicating CN substitution reduces the electron density in the range of −2 to 2 eV. Large electron density on CuPc segment is advantage for CO_2RR reaction.

CuCOF			CuCOF-CN			Change of bader charge
Atomic number	Element	Bader charge	Atomic number	Element	Bader charge	
1	C	0.59784	1	C	−0.34203	−0.93987
2	C	0.59784	2	C	−0.33591	−0.93375
3	C	0.3899	3	C	−0.34191	−0.73181
4	C	0.38819	4	C	−0.33602	−0.72421
5	C	0.38819	5	C	0.67422	0.28603
6	C	0.3899	6	C	0.67433	0.28443
7	C	0.59785	7	C	0.67422	0.07637
8	C	0.59785	8	C	0.67433	0.07648
9	C	0.00882	9	C	0.64228	0.63346
10	C	0.00882	10	C	0.64225	0.63343
11	C	0.00882	11	C	0.64223	0.63341
12	C	0.00882	12	C	0.64228	0.63346
13	C	0.00882	13	C	0.64227	0.63345
14	C	0.00882	14	C	0.64223	0.63341
15	C	0.00882	15	C	0.64223	0.63341
16	C	0.00882	16	C	0.64226	0.63344
17	C	−0.10487	17	C	−1.00724	−0.90237
18	C	−0.10487	18	C	−0.09079	0.01408
19	C	−0.10487	19	C	−0.09079	0.01408
20	C	0.10195	20	C	−1.00724	−1.10919
21	C	0.10196	21	C	−1.00724	−1.1092
22	C	0.10196	22	C	−0.09079	−0.19275
23	C	0.10196	23	C	−1.00724	−1.1092
24	C	−0.10487	24	C	−0.09079	0.01408
25	C	0.59277	25	C	−0.38101	−0.97378
26	C	0.39143	26	C	−0.38116	−0.77259
27	C	0.59277	27	C	−0.38116	−0.97393
28	C	0.39143	28	C	−0.38101	−0.77244
29	C	0.59278	29	C	0.58038	−0.0124
30	C	0.39144	30	C	0.58022	0.18878
31	C	0.39144	31	C	0.58037	0.18893
32	C	0.59278	32	C	0.58022	−0.01256
33	C	0.99682	33	C	1.37397	0.37715
34	C	0.99682	34	C	1.37433	0.37751
35	C	0.99682	35	C	1.37397	0.37715
36	C	0.99682	36	C	1.37397	0.37715
37	C	0.99682	37	C	1.37436	0.37754
38	C	0.99682	38	C	1.37436	0.37754
39	C	0.99682	39	C	1.374	0.37718
40	C	0.99682	40	C	1.37436	0.37754
41	C	−0.01794	41	C	1.2717	1.28964
42	C	−0.01794	42	C	1.2717	1.28964
43	C	−0.01793	43	C	1.27171	1.28964
44	C	−0.01794	44	C	1.2717	1.28964
45	Cu	1.1009	49	Cu	0.9131	−0.1878
46	H	0.070138	50	H	0.356329	0.286191
47	H	0.07014	51	H	0.356392	0.286252
48	H	0.070142	52	H	0.356217	0.286075
49	H	0.070137	53	H	0.356631	0.286494
50	H	0.070138	54	H	0.356769	0.286631
51	H	0.070143	55	H	0.356355	0.286212
52	H	0.070143	56	H	0.356657	0.286514
53	H	0.070141	57	H	0.356594	0.286453
58	N	−1.13474	62	N	−1.35308	−0.21834
Continued						

CuCOF			CuCOF-CN			Change of bader charge
Atomic number	Element	Bader charge	Atomic number	Element	Bader charge	
59	N	−1.13474	63	N	−1.35302	−0.21828
60		−1.13474	64	N	−1.35304	−0.2183
61	N	−1.13474	65	N	−1.35295	−0.21821
62		−1.23937	66	N	−1.49621	−0.25684
63	N	−1.23937	67	N	−1.49621	−0.25684
64		−1.23937	68	N	−1.49621	−0.25684
65	N	−1.23937	69	N	−1.49621	−0.25684
66	O	−1.05733	70	O	−1.19894	−0.14161
67	O	−1.05733	71	O	−1.19894	−0.14161
68	O	−1.05733	72	O	−1.19894	−0.14161
69	O	−1.05733	73	O	−1.19894	−0.14161
70	O	−1.05733	74	O	−1.19894	−0.14161
71	O	−1.05733	75	O	−1.19894	−0.14161
72	O	−1.05733	76	O	−1.19894	−0.14161
73	O	−1.05733	77	O	−1.19894	−0.14161
54	H	0.111745	45	C	0.7974	
55	H	0.111748	46	C	0.7974	
56	H	0.111757	47	C	0.7974	
57	H	0.111753	48	C	0.7974	
78			58		−1.2327	
79			59	N	−1.23243	
80			60	N	−1.23239	
81			61	N	−1.23252	

Table 2. Calculated bader charge (in e) on each atom of CuCOF and CuCOF-CN (see Fig. 1 for atomic label).

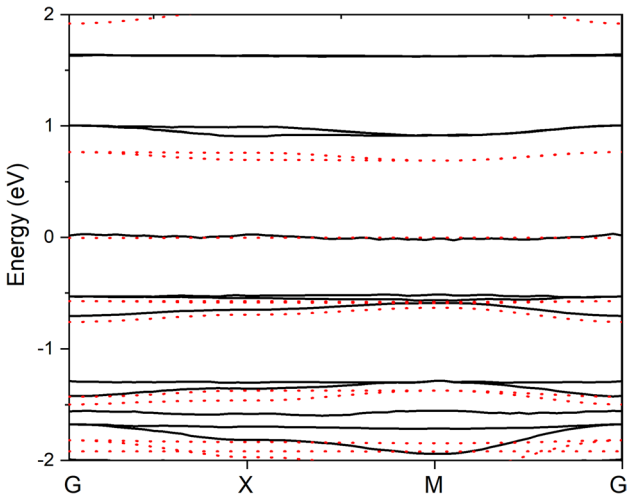

Fig. 2. Projected band structure of CuCOF (red dot line) and CuCOF-CN (black line).

CO2 RR

Figure 4 shows the free energy diagram of CO_2 RR on CuCOF and CuCOF-CN surface at U = 0 V. The structures of the main intermediates are given in Fig. 5. For both catalysts, the formation of *COOH is the rate determine step, with reaction energy of 1.75 and 1.78 eV for CuCOF and CuCOF-CN, respectively. The smaller reaction energy for CuCOF than CuCOF-CN indicates that changing CN groups to H is advantage for CO_2 RR. The desorption of CO need very small energy of only 0.13 and 0.14 eV for CuCOF and CuCOF-CN, respectively. The smaller reaction energy for CO desorption in CuCOF comparing to CuCOF-CN is also advantage for the whole CO_2 RR process. The different free energy of the intermediates for CuCOF and CuCOF-CN could be explained from the main structure parameter of the intermediates. The Cu-C distance of $*CO_2$ for CuCOF is shorter than that for CuCOF-CN (Fig. 5), well explaining the better stability of the former than the latter. Similarly, the longer Cu-C distance of *CO for CuCOF than CuCOF-CN reasons the less stable fact for the former than the latter.

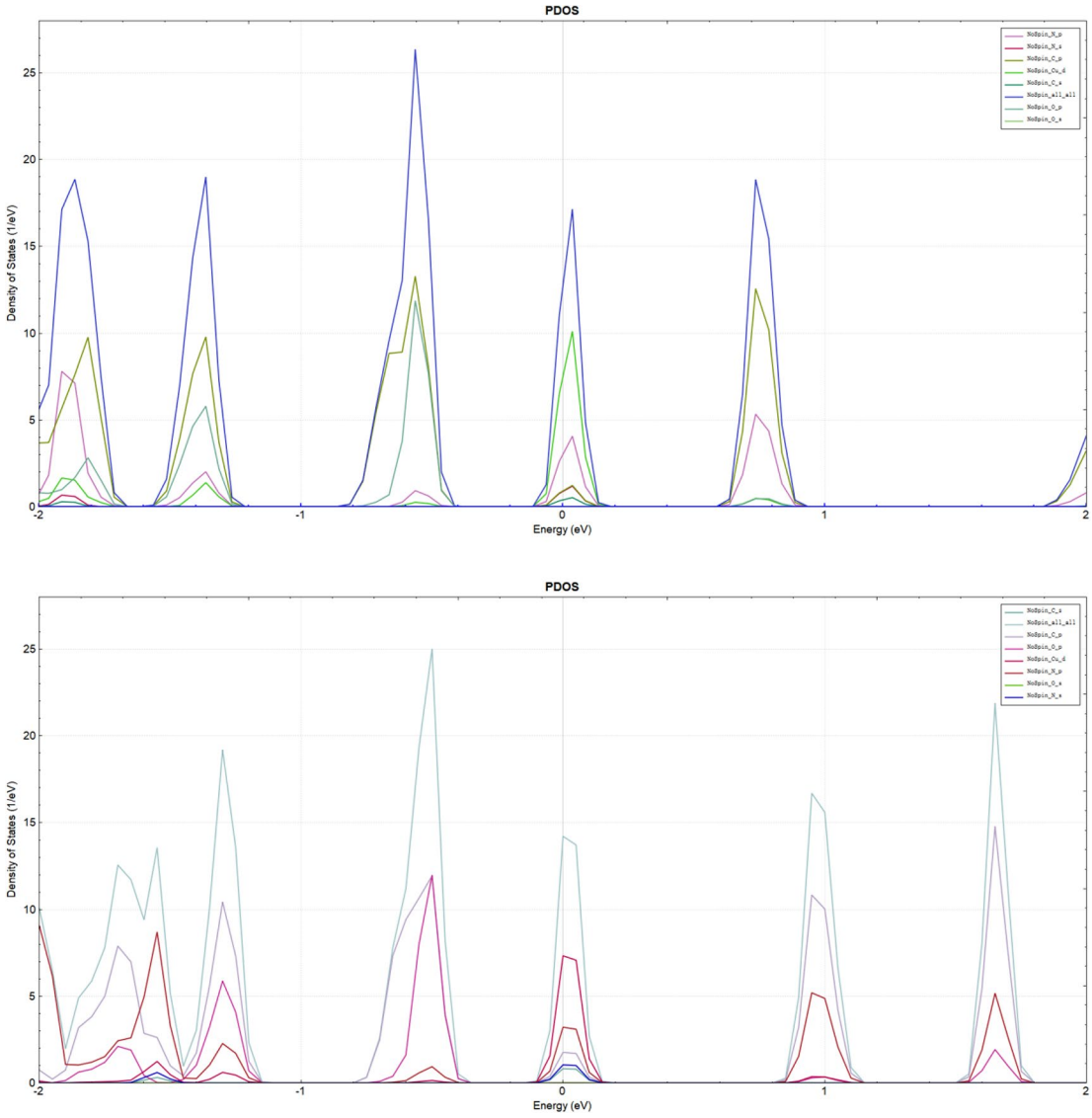

Fig. 3. Projected density of states of CuCOF (top) and CuCOF-CN (bottom).

Though the Cu-C length of *COOH for CuCOF is slightly longer than that of CuCOF-CN, the more positive charge of Cu in the former than the latter render CuCOF-COOH more stable than CuCOF-CN-COOH.

Conclusion

The crystal structures, electronic properties, and CO_2RR performance of CuCOF and CuCOF-CN were comparatively studied through first principle calculations. CuCOF was found to have reduced crystal unit size, more positive charge on Cu, smaller band gap, and lower reaction barrier for CO_2 RR, in comparing with CuCOF-CN. The good CO_2 RR catalytic performance and lower poisonousness for CuCOF than CuCOF-CN renders it good potential electrocatalyst with good environment friendliness.

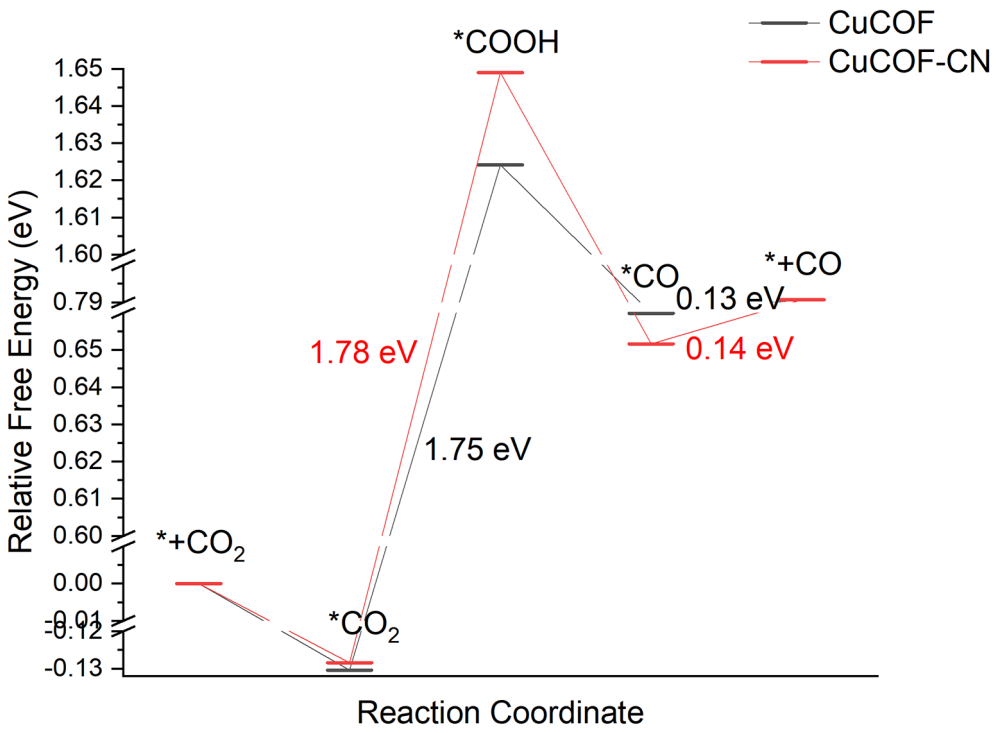

Fig. 4. The free energy diagram of CO_2RR on CuCOF (black) and CuCOF-CN (red) at U = 0 V.

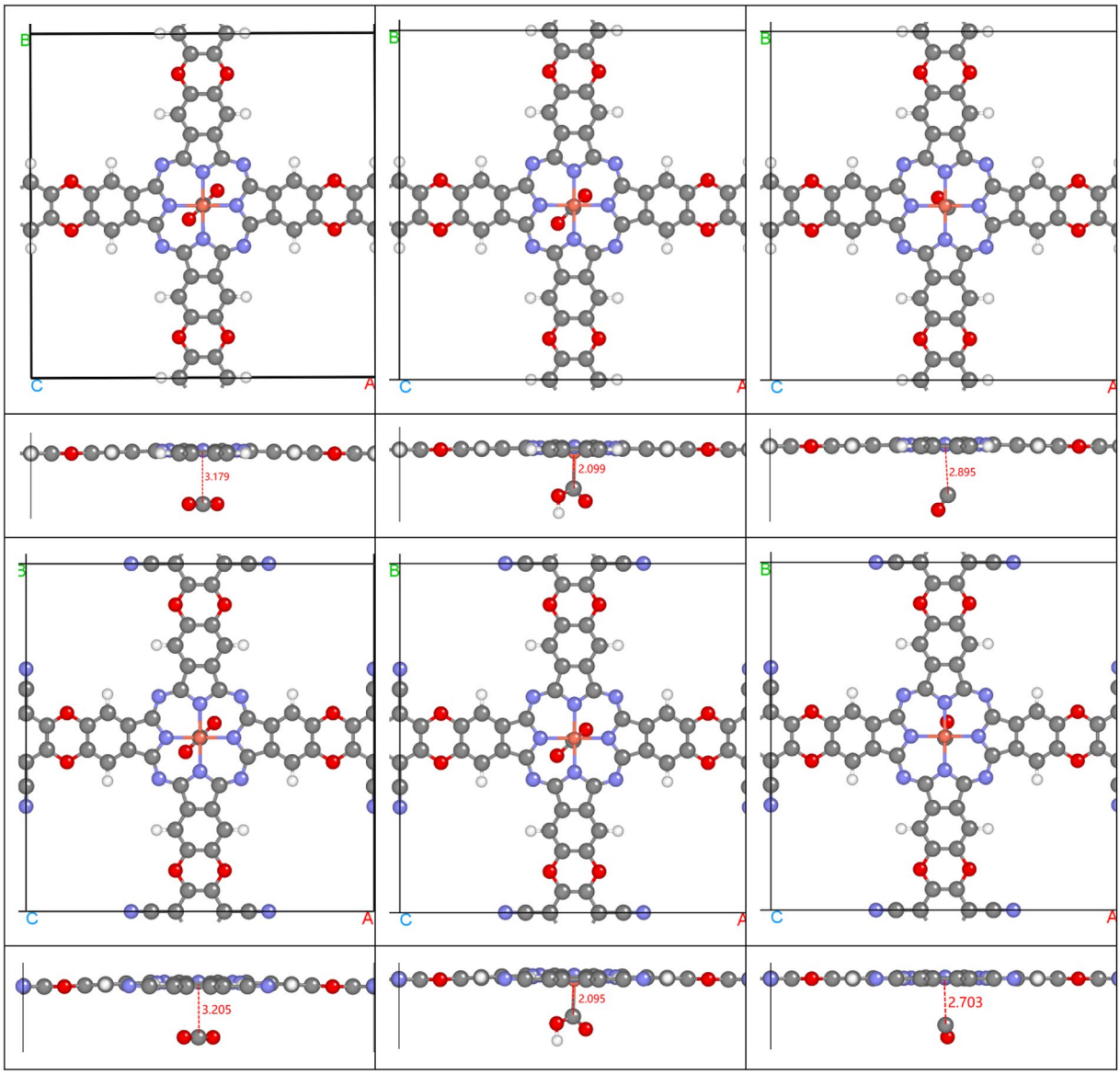

Fig. 5. Optimized crystal structure of the intermediates (*CO_2, left; *COOH, middle; *CO, right; * being the catalyst) during CO_2 RR with CuCOF (top two lines for top and side views, respectively) and CuCOF-CN (bottom two lines) as catalyst. (Red: O, gray: C, blue: N, white: H, coral: Cu).

Data availability

Data availability The data of this work including the input and output calculation files are available upon requirement from the corresponding authors.

Received: 21 July 2024; Accepted: 11 November 2024
Published online: 16 November 2024

References

1. Forkel, M. et al. Enhanced seasonal CO2 exchange caused by amplified plant productivity in northern ecosystems. *Science*. **351**, 696–699 (2016).
2. Seneviratne, S. I., Donat, M. G., Pitman, A. J., Knutti, R. & Wilby, R. L. Allowable CO2 emissions based on regional and impact-related climate targets. *Nature*. **529**, 477–483 (2016).
3. Varghese, O. K., Paulose, M., LaTempa, T. J. & Grimes, C. A. High-rate solar photocatalytic conversion of CO2 and water vapor to hydrocarbon fuels. *Nano Lett.* **9**, 731–737 (2009).
4. Liu, B. et al. Phosphorus-Doped Graphitic Carbon Nitride nanotubes with amino-rich surface for efficient CO2 capture, enhanced photocatalytic activity, and product selectivity. *ACS Appl. Mater. Interfaces*. **10** (4), 4001–4009 (2018).
5. Wang, W. H., Himeda, Y., Muckerman, J. T., Manbeck, G. F. & Fujita, E. CO 2 hydrogenation to formate and methanol as an alternative to photo- and Electrochemical CO 2 reduction. *Chem. Rev.* **115** (23), 12936–12973. https://doi.org/10.1021/acs.chemrev.5b00197 (2015).

6. Wang, T. et al. Central Site Regulation of Cobalt Porphyrin Conjugated polymer to give highly active and selective CO2 reduction to CO in aqueous solution. *Appl. Catal. B Environ.* **291**, 120128. https://doi.org/10.1016/j.apcatb.2021.120128 (2021).
7. Shen, J. et al. Electrocatalytic Reduction of Carbon Dioxide to Carbon Monoxide and methane at an immobilized cobalt protoporphyrin. *Nat. Commun.* **6** (1), 8177. https://doi.org/10.1038/ncomms9177 (2015).
8. Shen, J., Kolb, M. J., Göttle, A. J. & Koper, M. T. M. DFT Study on the mechanism of the Electrochemical Reduction of CO 2 catalyzed by Cobalt Porphyrins. *J. Phys. Chem. C.* **120** (29), 15714–15721. https://doi.org/10.1021/acs.jpcc.5b10763 (2016).
9. Wang, Y. R. et al. Oriented Electron Transmission in Polyoxometalate-Metalloporphyrin Organic Framework for highly selective electroreduction of CO2. *Nat. Commun.* **9** (1), 4466. https://doi.org/10.1038/s41467-018-06938-z (2018).
10. Vasileff, A., Zheng, Y. & Qiao, S. Z. Carbon solving Carbon's problems: recent progress of Nanostructured Carbon-based catalysts for the Electrochemical Reduction of CO 2. *Adv. Energy Mater.* **7** (21). https://doi.org/10.1002/aenm.201700759 (2017).
11. Elgrishi, N., Chambers, M. B., Wang, X. & Fontecave, M. Molecular polypyridine-based metal complexes as catalysts for the reduction of CO 2. Chem. *Soc. Rev.* **46** (3), 761–796. https://doi.org/10.1039/C5CS00391A (2017).
12. Nitopi, S. et al. Progress and perspectives of Electrochemical CO 2 reduction on copper in Aqueous Electrolyte. *Chem. Rev.* **119** (12), 7610–7672. https://doi.org/10.1021/acs.chemrev.8b00705 (2019).
13. Wei, X. et al. Highly selective reduction of CO 2 to C 2+hydrocarbons at Copper/Polyaniline Interfaces. *ACS Catal.* **10** (7), 4103–4111. https://doi.org/10.1021/acscatal.0c00049 (2020).
14. Ma, W. et al. Electrocatalytic reduction of CO2 to Ethylene and ethanol through hydrogen-assisted C–C coupling over fluorine-modified copper. *Nat. Catal.* **3** (6), 478–487. https://doi.org/10.1038/s41929-020-0450-0 (2020).
15. Chen, D. et al. A Tandem Strategy for Enhancing Electrochemical CO 2 reduction activity of single-atom Cu-S 1 N 3 catalysts via integration with Cu Nanoclusters. *Angew Chemie Int. Ed.* **60** (45), 24022–24027. https://doi.org/10.1002/anie.202109579 (2021).
16. Yang, B. et al. CO 2 electroreduction to Multicarbon products via Synergistic Electric–Thermal Field on Copper Nanoneedles. *J. Am. Chem. Soc.* **144** (7), 3039–3049. https://doi.org/10.1021/jacs.1c11253 (2022).
17. Creissen, C. E. & Fontecave, M. Keeping Sight of copper in single-atom catalysts for Electrochemical Carbon Dioxide Reduction. *Nat. Commun.* **13** (1), 2280. https://doi.org/10.1038/s41467-022-30027-x (2022).
18. Han, N. et al. Supported Cobalt Polyphthalocyanine for High-Performance Electrocatalytic CO2 reduction. *Chem. 2017*, **3** (4), 652–664. https://doi.org/10.1016/j.chempr.2017.08.002
19. Wu, Y., Jiang, Z., Lu, X., Liang, Y. & Wang, H. Domino electroreduction of CO2 to methanol on a Molecular Catalyst. *Nature*. **575** (7784), 639–642. https://doi.org/10.1038/s41586-019-1760-8 (2019).
20. Sun, L. et al. Conjugated N 4 -Macrocyclic Cobalt Complex for Heterogeneous Electrocatalytic CO_2 reduction with high activity. *Angew Chemie Int. Ed.* **59** (39), 17104–17109. https://doi.org/10.1002/anie.202007445 (2020).
21. Wang, R., Kapteijn, F. & Gascon, J. Engineering Metal–Organic frameworks for the Electrochemical reduction of CO 2: a Minireview. *Chem. – Asian J.* **14** (20), 3452–3461. https://doi.org/10.1002/asia.201900710 (2019).
22. Wang, J., Huang, X., Xi, S., Xu, H. & Wang, X. Axial Modification of Cobalt Complexes on heterogeneous surface with enhanced Electron transfer for Carbon Dioxide Reduction. *Angew Chemie Int. Ed.* **59** (43), 19162–19167. https://doi.org/10.1002/anie.202008759 (2020).
23. Zhang, X. et al. Highly selective and active CO2 reduction Electrocatalysts based on Cobalt Phthalocyanine/Carbon Nanotube Hybrid structures. *Nat. Commun.* **8** (1), 14675. https://doi.org/10.1038/ncomms14675 (2017).
24. Huang, N. et al. Stable and conductive metallophthalocyanine Framework for Electrocatalytic Carbon Dioxide Reduction in Water. *Angew Chemie Int. Ed.* **59** (38), 16587–16593. https://doi.org/10.1002/anie.202005274 (2020).
25. Lu, M. et al. Stable dioxin-linked Metallophthalocyanine Covalent Organic frameworks (COFs) as photo-coupled electrocatalysts for CO 2 reduction. *Angew Chemie Int. Ed.* **60** (9), 4864–4871. https://doi.org/10.1002/anie.202011722 (2021).
26. Diercks, C. S., Liu, Y., Cordova, K. E. & Yaghi, O. M. The role of Reticular Chemistry in the design of CO2 reduction catalysts. *Nat. Mater.* **17** (4), 301–307. https://doi.org/10.1038/s41563-018-0033-5 (2018).
27. Diercks, C. S. & Yaghi, O. M. The atom, the Molecule, and the Covalent Organic Framework. *Science*. **355** (6328), eaal1585. https://doi.org/10.1126/science.aal1585 (2017).
28. Qiu, X. F. et al. A stable and conductive covalent Organic Framework with isolated active sites for highly selective electroreduction of Carbon Dioxide to acetate. Angew. *Chemie - Int. Ed.* **61** (36), e202206470. https://doi.org/10.1002/anie.202206470 (2022).
29. Yang, X. et al. Ionothermal synthesis of fully conjugated covalent Organic frameworks for High-Capacity and Ultrastable Potassium-Ion batteries. *Adv. Mater.* **34** (50), 2207245. https://doi.org/10.1002/adma.202207245 (2022).
30. Liu, Q. et al. Universal Synthesis of Metallophthalocyanine Covalent Organic frameworks as Ultra-sensitive Multifaceted Electrochemical Sensor. *Sci. China Chem.* **67** (6), 2092–2101. https://doi.org/10.1007/s11426-024-1998-5 (2024).
31. Hongzhiwei, Technology & China Device Studio, Version 2023A, Available online: (2023). https://cloud.hzwtech.com/web/product-service?id=6
32. Blöchl, P. E. Projector augmented-wave method. *Phys. Rev. B.* **50** (24), 17953 (1994).
33. Perdew, J. P., Burke, K. & Ernzerhof, M. Generalized gradi- ent approximation made simple. *Phys. Rev. Lett.* **77**, 3865–3868. https://doi.org/10.1103/PhysRevLett.77.3865 (1996).
34. Grimme, S., Ehrlich, S. & Goerigk, L. Effect of the damping function in Dispersion Corrected Density Functional Theory. *J. Comput. Chem.* **32** (7), 1456–1465. https://doi.org/10.1002/jcc.21759 (2011).

Acknowledgements

Financial supports from National Natural Science Foundation of China (52460023, 22478366), Natural Science Foundation of Shandong Province (2023TSGC0018), Natural Science Foundation of Jianxi Province (20224BAB213031), and Dezhou University (2023xjrc111) are acknowledged. This work was also supported by funding from Shandong Provincial Key Laboratory of Monocrystalline Silicon Semiconductor Materials and Technology (2023KFKT012). We gratefully acknowledge HZWTECH for providing computation facilities.

Author contributions

Yuexing Zhang conceived the idea, performed the DFT calculations and wrote the original draft. Junhao Peng, Guangsong Zhang, and Xingguo Zhang performed addition DFT calculations, analyzed calculation data, and revised the manuscript. Shuai Zhang, Qing Li, Guanfeng Tian, Xiaoli Wang, and Ping Wu discussed the results and revised the manuscript. Yuexing Zhang and Xue-Li Chen supervised and directed the projects and revised the manuscript. All authors reviewed the manuscript.

Declarations

Competing interests

The authors declare no competing interests.

Additional information

Correspondence and requests for materials should be addressed to Y.Z. or X.-L.C.